

Efficient Worst Case “1-Cosine” Gust Loads Prediction

(Received: Jan. 13, 2012. Revised: Aug. 2, 2012. Accepted: Aug. 29, 2012)

Abstract

This paper describes several approaches aiming to significantly reduce the amount of time required to determine the worst case gust loads for aircraft. A number of Design of Experiments, surrogate modeling and optimization techniques are applied in order to determine meta-models encompassing the entire flight envelope and different fuel cases using only a few test points. All of the methodologies are compared on data from a simple, assumed modes, free-free aircraft model with 5 “interesting quantities”, and are shown to determine accurate predictions of the worst gust case with far fewer gust response calculations than a conventional Monte-Carlo approach.

H. H. KHODAPARAST¹
G. GEORGIU²
J. E. COOPER³
L. RICCOBENE⁴
S. RICCI⁴
G. A. VIO⁵
P. DENNER⁶

1. Introduction

Unsteady loads calculations play an important part across much of the design and development of an aircraft, and have an impact upon the concept and detailed structural design, aerodynamic characteristics, weight, flight control system design, control surface design and performance. They determine the most extreme stress levels and estimate fatigue damage and damage tolerance for a particular design. For this purpose, load cases due to dynamic gusts and manoeuvres are applied to detailed structural models [23, 3, 12, 15] in order to determine the worst values for a range of different Interesting Quantities (IQs) e.g. load factors, shear stresses, etc. There may be 1000s of IQs that need to be considered.

The certification of large commercial aircraft is covered by the EASA CS-25 (Certification Specifications) or FAR-25 documents. A range of load cases that has to be accounted for are described and are a primary prerequisite for assuring structural integrity over the operating environment of the aircraft. Loads requirements are defined in the context of the design envelope shown in Figure 1. Certification specifications require that enough points, on or within the boundaries of the design envelope, are investigated to ensure that the most extreme loads for each part of the aircraft structure are identified. In this context, the design envelope encompasses the respective ranges of permitted mass/centre of mass envelopes.

The flight conditions and manoeuvres, which provide the largest aircraft loads, are not known a-priori. Therefore the aerodynamic and inertial forces are calculated at a large number of conditions to give an estimate of the maximum loads, and hence stresses and deflections, that the structure of the detailed aircraft design will experience in service. Table 1 shows an estimate of the number of conditions that are typically required in the analysis of a large civil aircraft.

¹ Centre for Engineering Dynamics, School of Engineering, University of Liverpool
Liverpool, United Kingdom

² Virtual Engineering Centre, School of Engineering, University of Liverpool
Liverpool, United Kingdom

³ Department of Aerospace Engineering, University of Bristol
Bristol, United Kingdom

⁴ Department of Aerospace Engineering, Politecnico di Milano
Milano, Italy

⁵ Department of Mechanical and Aerospace Engineering, University of Sydney
Sydney, Australia

⁶ Airbus Operations Ltd, Filton,
Bristol, United Kingdom

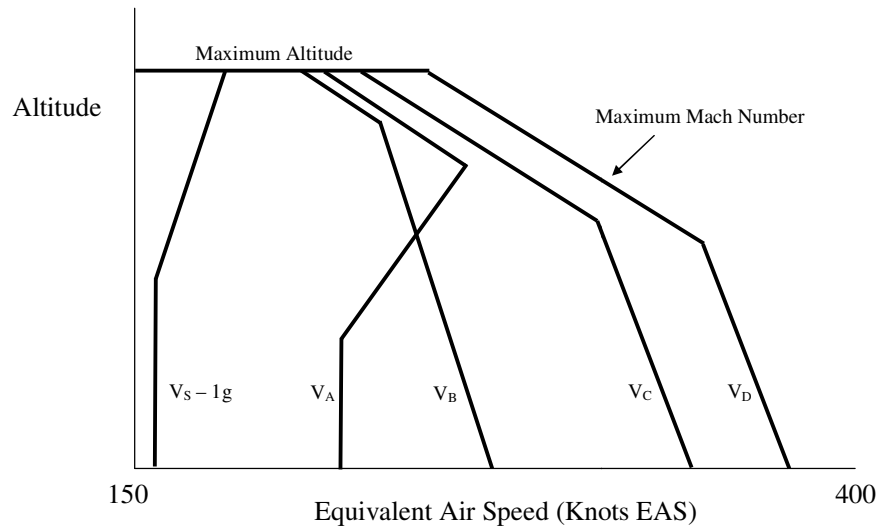


Figure 1: Flight Envelope Design Speed vs Altitude [23].

Table 1: Estimate of Number of Load Cases Required.

Number of points	Parameters
50	flights points (altitude and speed)
100	mass cases (loaded weight and weight distribution)
10	control surface configuration
50	manoeuvres and gusts (gradient length)
4	control laws
10,000,000	TOTAL NUMBER OF CASES REQUIRED

A simplistic estimate of the number of analyses required would multiply the numbers of conditions to give 10,000,000. Even with simplistic models of the aircraft behaviour this is an unfeasible number of separate simulations. However, engineering experience is used to identify the most likely critical loads conditions, meaning that approximately 100,000 simulations are required for conventional aircraft configurations. Furthermore, these analyses have to be repeated every time that there is an update in the aircraft structure. Within the modern civil airframe industry, each of these loads calculation cycles takes a considerable time.

A further important point is that the new aircraft configurations that will be vital to meet environmental performance targets e.g. the 2020 vision, are likely to possess design envelope boundaries and therefore critical loads cases, that are very different from those previously found on conventional aircraft. If the aerospace industry moves to novel configurations there will be a longer product development cycle as it will not be possible to rely on engineering judgement from similar aircraft. Engineering experience, that is currently used to reduce the number of critical loads cases without compromising air safety, cannot be extended to novel configurations. This would mean a huge increase in the number of loads analyses that would be needed to ensure air safety for novel aircraft and hence very large increases in both design cost and turnaround time. This could result in a reluctance to move to new configurations unless the loads process cost can be brought back to the status quo which can only be achieved through reliance on modelling (which must be more accurate and rapid than is currently possible) and robust critical load identification in place of engineering judgement. Hence, there is a need to formalise the critical loads identification process so that there is neither a development cost penalty or a decrease in safety. Indeed, such a capability is crucial in enabling the aircraft design process to evolve so that more concepts can be explored and matured over shorter lead times.

The number of different flight conditions that need to be considered to assess the maximum loads that will be encountered by a civil aircraft is large and must be reduced. At present engineering experience is used to achieve a significant reduction for conventional aircraft geometries whose response can be calculated using assumptions of linearity. With the advent of non-linear control systems and new manufacturing techniques, even conventional aircraft are becoming increasingly nonlinear and the linearity assumption is becoming unacceptable. One of the aims of the FFAST project is to implement and assess the capabilities of a general methodology to minimize the number of flight conditions that are needed to characterise the whole parameter space for aircraft design through the use of optimisation and design of experiments methodologies. In addition, since gusts are often the most critical load case for structural design and also are the main fatigue loading source for the majority of the structure, fast and accurate methodologies will be developed to determine the worst case gust loads for a non-linear aircraft.

Currently, a preliminary selection of the most important cases needs to be made, generally based on the "worst case" approach and using a great deal of engineering experience to give an estimate of the maximum loads that the structure of the aircraft will experience in service [23, 15]. The prediction of linear gust responses is well-established and used in industry. The airworthiness regulations require that gust loads analysis is performed in both the time (critical high frequency responses) and frequency (critical low frequency responses) domains, considering both vertical and lateral gust patterns. In the time domain, an approach based upon tuned "1-Cosine" gusts has developed [23, 7, 9] which involves finding the particular time gust sequence that causes the worst (largest) response for each "Interesting Quantity" (IQ) such as load factor, root bending moment, shear force, etc. As explained above, the current process is very time consuming.

In this work, a number of different approaches are applied in order to speed up the gust loads prediction process through the efficient and accurate determination of the worst "1-Cosine" gust loads case. Surrogate modeling and optimization techniques are applied to determine the worst case loads across a range of different flight conditions (altitude, speed, fuel condition, centre of gravity position) to enable the global worst case to be found. The optimal sampling technique using the Kriging predictor is introduced and shown that it is capable of identifying the worst cases using much smaller number of samples which are needed for conventional sampling techniques such as Latin Hypercube Sampling (LHS) or Design of Experiments (DOE). The approaches are evaluated on a simple free-free aeroelastic model comprising of rigid body and flexible modes.

2. Worst Case "1-Cosine" Gust Response

A typical "1-cosine" gust is shown in Figure 2, with a maximum gust velocity of W_{g0} and the gust wavelength is L_g . Of interest is the gust wavelength L_g that produces the greatest maximum and minimum response of particular "interesting quantities" (IQs), e.g. wingtip deflection, centre of gravity acceleration, wing root bending moment, etc. For different gust gradients H (half the gust wavelength (m)), the maximum gust velocity W_{g0} (m/s) is defined as [23]

$$W_{g0} = W_{ref} \left(\frac{H}{106.17} \right)^{1/6} \quad (1)$$

and it can be seen in Figure 3 how the maximum gust velocity increases with wavelength. The reference gust velocity W_{ref} reduces linearly from 17.07 m/s EAS at sea level to 13.41m/s EAS at 4572m (15000ft), and then again to 6.36 m/s EAS at 18288 m (60000ft).

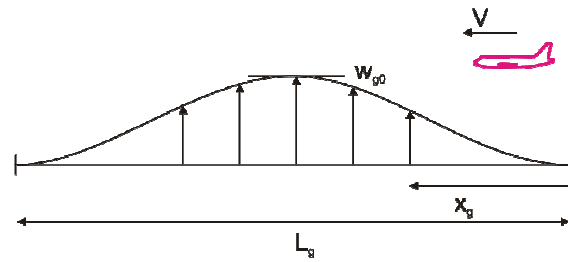


Figure 2: "1-Cosine Gust" [23].

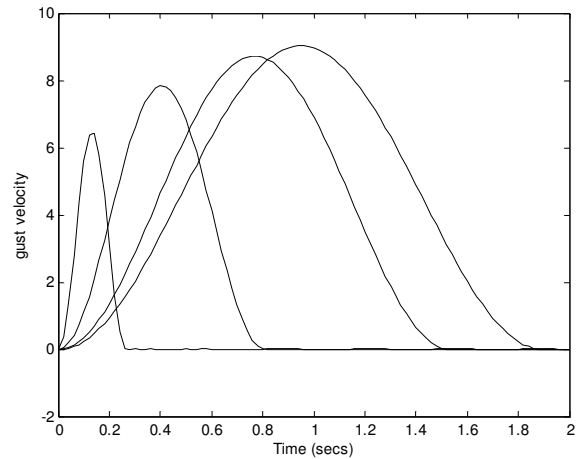


Figure 3: Varying Amplitude Gusts Following Scaling Law.

3. Aeroelastic Model

As an initial test bed for the gust load prediction methods, the three-dimensional NLR 5 DOF model [22] was used. The model is shown in Figure 4, with the structure modelled with a series of linear beam elements and lumped masses, and aerodynamic strip theory with downwash tail effects included. The model is symmetrical, as a result for the vertical gust case there are two rigid body modes (heave and pitch) and three flexible modes (wing root bending, wing root torsion and rear fuselage bending). Additionally, it is possible to define the structural properties (dimensions, mass distribution, inertia, stiffness) of the aircraft, and also the gust input. In this work, the discrete gust shape of the form "1-Cosine" was considered. The response of five IQs (load factor, wing root shear force, wing root bending moment, wing root torsion moment, tail root shear force) can be determined; a typical example of input gust and response for the IQs is shown in Figure 5.

For a particular aircraft configuration (flight condition, size, mass distribution, etc) a range of different wave length "1-Cosine" gusts can be applied, resulting in the envelopes shown in Figure 6 of the largest maximum and minimum responses for the five IQs. It can be seen that the various maxima and minima do not occur at the same gust length, and these will change depending upon the flight condition, mass distribution, centre of gravity position, etc.

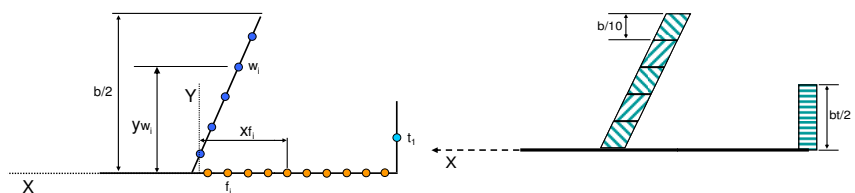


Figure 4: Structural and Aerodynamic Elements in the NLR model.

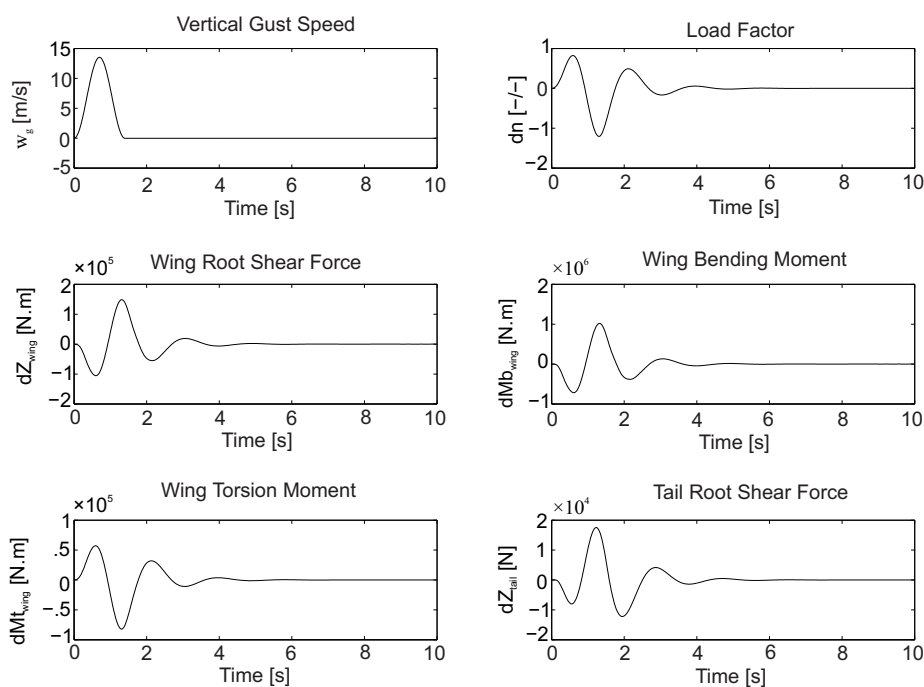


Figure 5: Typical IQ responses to "1-Cosine" Vertical Gust Input (top left).

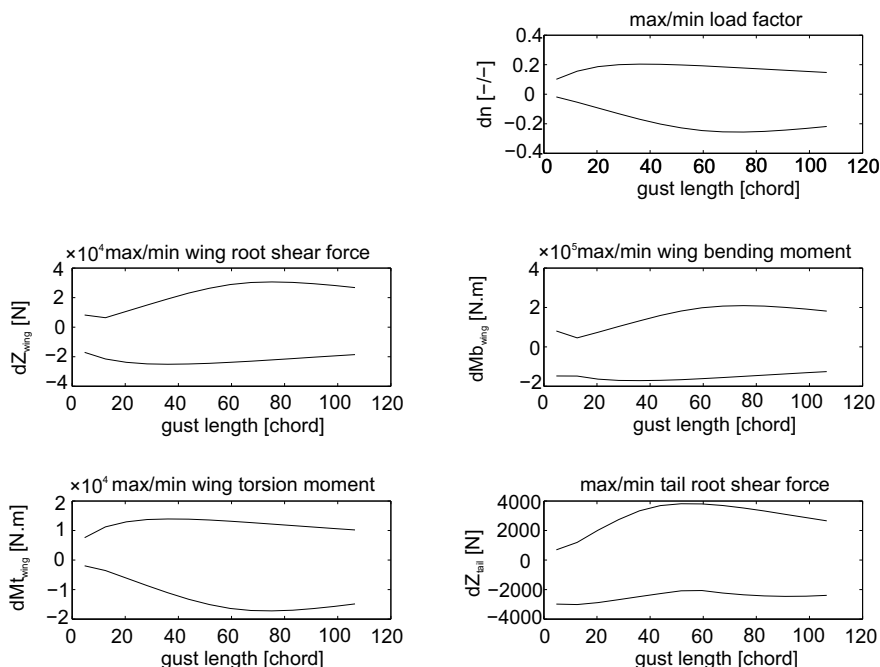


Figure 6: Maximum and Minimum Envelopes for the IQs for Different Gust Lengths.

4. Surrogate Modelling Approaches

A complete description of metamodeling techniques and their use in modern industrial applications is beyond the scope of this paper [5]. We would like just to introduce a few basic concepts allowing to reader to clearly understand how these techniques are used inside the FFAST project to reduce the time required for the calculation of aircraft gust response. The process for the definition of a metamodel, to be adopted for the simulation of the aircraft gust response can be synthesized in the following three steps: Sampling, Metamodeling and Model Validation. These steps will be briefly detailed in the following paragraphs.

The main scope of Sampling is to get the maximum amount of information related to the system behaviour with the minimum effort in terms of computation time, so with the minimum number of samples. The design space is sampled and the available sampling techniques differ in how they distribute these samples into the design domain. The classical experimental designs originated from the theory of Design of Experiments when physical experiments are conducted. In this category it is worth mentioning the factorial or fractional factorial [17], central composite design (CCD) [17, 1] and Box-Behnken [17] approaches. In the case that the maximum or minimum regions of the fitted surfaces are of interest optimal sampling method [14] can be used. In this method the samples are mostly taken from the regions around maximum/minimum values of the function.

Traditionally, Metamodeling originated from the classical Design of Experiments (DOE) theory, where polynomial functions are used to build-up response surfaces, or metamodels. The polynomial coefficients are determined in a least square sense, so the effect is to smooth the peaks of the real behaviour. Sacks et al. [21, 20] proposed the use of a stochastic model, called Kriging [2], to treat the deterministic computer response as a realization of a random function with respect to the actual system response. Neural networks have also been applied in generating response surfaces for system approximation [18]. Among the other types of techniques available are the Radial Basis Functions (RBF) [4, 6] and Multivariate Adaptive Regression Splines (MARS) [8] approaches. It is difficult to define “a-priori” the best metamodeling technique. Here it was decided to limit the investigation to only two approaches, the Kriging and Radial Basis Functions.

4.1 Radial Basis Function (RBF)

The Radial Basis Function method is an interpolating scheme, originally developed by Dyn et al. [4], used to describe the behavior of non-linear functions once known a set of N sample points. The approximation is obtained by a linear combination of radial functions, each one centered in one of the sample points. Among the most frequently adopted RBF are

$$\textit{linear} \quad \phi(r_{x-x_n}) = r_{x-x_n} \quad (2)$$

$$\textit{cubic} \quad \phi(r_{x-x_n}) = (r_{x-x_n})^3 \quad (3)$$

$$\textit{Gaussian} \quad \phi(r_{x-x_n}) = e^{-(r_{x-x_n})^2} \quad (4)$$

where the distance between the generic point x and the sample points x_n is

$$r_{x-x_n} = \|x - x_n\|^2 \quad (5)$$

4.2 Kriging predictor

The introduction of the Kriging approach [2] is due to the observation that many computer analysis codes are deterministic and therefore not subject to

measurement error, consequently the usual measures of uncertainty derived from least-squares residuals have no obvious meaning.

To construct the Kriging meta model, it is assumed that n_s vectors of independent input parameters $\mathbf{X} = [\mathbf{x}^{(1)} \mathbf{x}^{(2)} \dots \mathbf{x}^{(n_s)}]$ with $\mathbf{x}^{(i)} \in \mathfrak{R}^{m \times 1}$ are selected by using a sampling method and the corresponding output parameters $\mathbf{Y} = [\mathbf{y}^{(1)} \mathbf{y}^{(2)} \dots \mathbf{y}^{(n_s)}]$ with $\mathbf{y}^{(i)} \in \mathfrak{R}^{n \times 1}$ are calculated using deterministic analysis of system. Then a universal Kriging predictor for the output data consists of a second order polynomial function is expressed as [21],

$$\begin{aligned} \hat{y}_i &= \beta_{0,i} + \sum_{k=1}^m \beta_{k,i} x_k + \sum_{k=1}^m \beta_{kk,i} x_k^2 + \sum_{k < l} \sum_{l=2}^m \beta_{kl,i} x_k x_l + \epsilon_i(\mathbf{x}) \\ &= \beta_{0,i} + \mathbf{b}_i^T \mathbf{x} + \frac{1}{2} \mathbf{x}^T \mathbf{B}_i \mathbf{x} + \epsilon_i(\mathbf{x}) \end{aligned} \quad (6)$$

where $\beta_{\bullet,i}$ are regression coefficients, $\mathbf{b}_i = [\beta_{1,i} \beta_{2,i} \dots \beta_{p,i}]_{m \times 1}^T$,

$$\mathbf{B}_i = \begin{bmatrix} 2\beta_{11,i} & \beta_{12,i} & \cdot & \cdot & \cdot & \beta_{1m,i} \\ & 2\beta_{22,i} & \cdot & \cdot & \cdot & \beta_{2m,i} \\ & & \cdot & & & \cdot \\ & & & \cdot & & \cdot \\ & \text{sym.} & & & & \cdot \\ & & & & & 2\beta_{mm,i} \end{bmatrix}_{m \times m}$$

and $\epsilon_i(\mathbf{x})$ is a random function having zero-mean and covariance,

$$\text{cov}(\epsilon_i(\mathbf{x}), \epsilon_i(\mathbf{x}^{(h)})) = \sigma_i^2 C_i(\mathbf{x}, \mathbf{x}^{(h)}) \quad (7)$$

where σ_i^2 is the variance of the i^{th} output data and C_i is the correlation function between untried input parameter \mathbf{x} and one of the design sample $\mathbf{x}^{(h)}$, $h = 1 : n_s$. A suitably chosen correlation function may improve the quality of fit as explained below. The random function represents the error and since our application is to fit a regression model on a deterministic computer code, any lack of fit will be due entirely to modeling error (incomplete set of regression terms), not measurement error or noise [14]. Hence, the random function in Eq. (6) becomes a function of the system parameters \mathbf{x} and the errors of the output predictor in Eq. (6) are correlated. The correlation function of the prediction errors is assumed to be related inversely to the distance between the corresponding points in the output [14]. The closer the points in space, the greater the correlation between the error terms. Because the components of input parameters are statistically independent, one may calculate the correlation function between the input parameters as [21],

$$C_i(\mathbf{x}, \mathbf{x}^{(h)}) = \prod_{j=1}^p C_{j,i}(x_j, x_j^{(h)}) \quad (8)$$

Different types of correlation functions have been introduced in [13] and [16]. The choice of correlation function depends on underlying behavior of the true response. However, this underlying behavior is often not readily apparent, in which case the following correlation function may be used,

$$C_{j,i}(x_j, x_j^{(h)}) = \exp\left(-\zeta_{j,i} |x_j - x_j^{(h)}|^{\nu_i}\right) \quad 1 \leq \nu_i \leq 2 \quad (9)$$

where $\zeta_{j,i}$ (the j^{th} term of the vector $\boldsymbol{\zeta}_i$) and ν_i are parameters of the correlation function at the i^{th} output. $\nu_i = 1$ gives an Ornstein-Uhlenbeck process which produces continuous paths but not very smooth. The case $\nu_i = 2$ produces infinity differentiable paths. Therefore the parameter ν_i is related to the smoothness of the function in x_j coordinates. As it is seen in Eq. (9), the correlation function is 1 when $x_j = x_j^h$ and its value reduces as the untried point

x_j is positioned further away from the h^{th} design point x_j^h . Since the predictor is unbiased at the observation point, a high level of confidence in the prediction of the outputs for the points which are close to the design samples can be achieved. The parameter $\zeta_{j,i}$ controls the importance of the j^{th} component. The calculation of correlation parameters is explained in detail in [14].

4.2.1 Optimal Sampling for the Kriging predictor

In many applications the maximum or minimum of the fitted surfaces are of interest and therefore it is beneficial to use an optimal sampling method in a way that samples are mostly taken from the regions around maximum/minimum values of the function. It is assumed that firstly n_s samples are taken from the space of parameters variations using Central Composite Design [17]. Then an estimate of the minimum/maximum value of the function is calculated based on the available samples as follows:

$$y_{max/min} = max/min (y^1, y^2, \dots, y^{n_s}) \quad (10)$$

As mentioned in section 4.2, the Kriging predictor at any point can be considered as a random variable given by the mean standard error. Viewed in this way, a probability can be calculated that the value at any point will be lower than the current minimum or upper than the current maximum. The expected improvement function (EIF) is then computed by weighting the possible improvements by these probability densities and is written as [14]

$$E[I(x)] = (f_{min} - \bar{y}) \Phi\left(\frac{f_{min} - \bar{y}}{s}\right) + s\phi\left(\frac{f_{min} - \bar{y}}{s}\right) \quad (11)$$

$$E[I(x)] = (\bar{y} - f_{max}) \left(1 - \Phi\left(\frac{f_{max} - \bar{y}}{s}\right)\right) + s\phi\left(\frac{f_{max} - \bar{y}}{s}\right) \quad (12)$$

where E is Expected value, \bar{y} is the mean value of Kriging predictor, Φ is the Gaussian cumulative distribution function, ϕ is the Gaussian probability distribution function, s is root of mean square error, f_{max} is maximum value of mean value of the Kriging predictor and f_{min} is the minimum value of mean value of the Kriging predictor. The expected improvement function (EIF) is calculated at all the points of the parameter space and the next samples are taken from the point having maximum EIF. The procedure continues until the maximum EIF falls below a specified threshold.

5. Results of NLR model

The effect of variation of 6 parameters on the response of 5 Interesting Quantities (IQs) for a typical "1-Cosine" gust is studied in this paper. The centre of gravity position behind nose of m.a.c. in wing chords $cxcg$, half aircraft mass m , airspeed V , altitude alt , half moment of inertia I and gust length L_g are assumed to be varied in the ranges shown in Table 2.

The output data are considered to be the maximum and minimum values of load factor, wing root shear force, wing root bending moment, wing root torsion moment and tail shear force. Two Meta models (RBF and Kriging) were constructed with the 6 input parameters (explained in Table 2) and the 10 output responses (explained in Table 2). As shown in the following sections different sampling techniques are used to construct the meta-models.

5.1 RBF Results

Two DOE techniques were evaluated for the definition of the sample points-Full Factorial and Latin Hypercube. A cubic RBF was calculated throughout. For the results shown here, the Factorial DOE approach used the levels defined in

Parameter	Description	Min	Max	Levels
$cxcg$	cg position in chord	0.1	0.2	3
m	aircraft mass (kg)	15000	25000	3
V	airspeed (TAS, m/s)	50	220	3
alt	altitude (m)	0	11000	4
H	Gust gradient (m)	9	107	5
I	Inertia term ($kg.m^2$)	0.3e6	1.3e6	3

Table 2: The DOE adopted for gust response metamodeling. The selected DOE corresponds to a total number of samples equal to 1800.

Description	R	RMSE	R
Description	% Factorial	% LHS	% LHS
IQ1	99.69	11.423	99.9
IQ2	99.59	8.860	99.83
IQ3	98.987	7.675	98.91
IQ4	99.04	8.944	99.47
IQ5	98.47	9.771	98.02
IQ6	99.11	7.518	99.2
IQ7	98.995	7.199	98.88
IQ8	99.18	9.821	99.44
IQ9	98.68	13.501	99.44
IQ10	98.16	8.564	98.33

Table 3: Correlation Factor Results for Factorial (1800) and Latin Hypercube (600) RBF fits.

where:

IQ1:	Max CoG Load Factor
IQ2:	Min CoG Load Factor
IQ3:	Max Wing Root Shear Force
IQ4:	Min Wing Root Shear Force
IQ5:	Max Wing Root Bending Moment
IQ6:	Min Wing Root Bending Moment
IQ7:	Max Wing Root Torsion Moment
IQ8:	Min Wing Root Torsion Moment
IQ9:	Max Tail Root Shear Force
IQ10:	Min Tail Root Shear Force

Table 2 with 1800 samples, whereas the LHS method used only 600 samples taken at 10 levels. Table 3 shows that good results can be obtained using relatively few test samples.

Figures 7 and 8 show correlation plots and response surfaces for the RBF-LHS fits. The quality of the fits is still good, although (understandably) the accuracy does start to degrade as the number of test points reduces.

5.2 Kriging Results

A generalised Kriging Meta model was constructed with the 6 input parameters and the 10 output responses introduced in section 5. Firstly three equally-spaced points are taken for each of $cxcg$, m , V , alt and 10 points for L_g (note that for this analysis the inertia term was taken as constant), resulting in the total of 810 samples. The variations of each output parameters in terms of variation of two input parameters (while the other three parameters are fixed at their mean values) were plotted and it was observed that there is a good agreement between the true surfaces and those surfaces obtained by Kriging predictor. For example, the variation of maximum wing root bending moment versus gust length and air velocity and the variation of minimum wing root torsion moment versus gust length and altitude are shown in Figures 9 and 10. The purpose of this part of work was to obtain a meta-model which is capable of representing the true values of 10 IQs within the whole space of variation for the input parameters. Therefore 810 samples were used to achieve this goal. However, if only maximum/minimum values of IQs are sought then the optimal

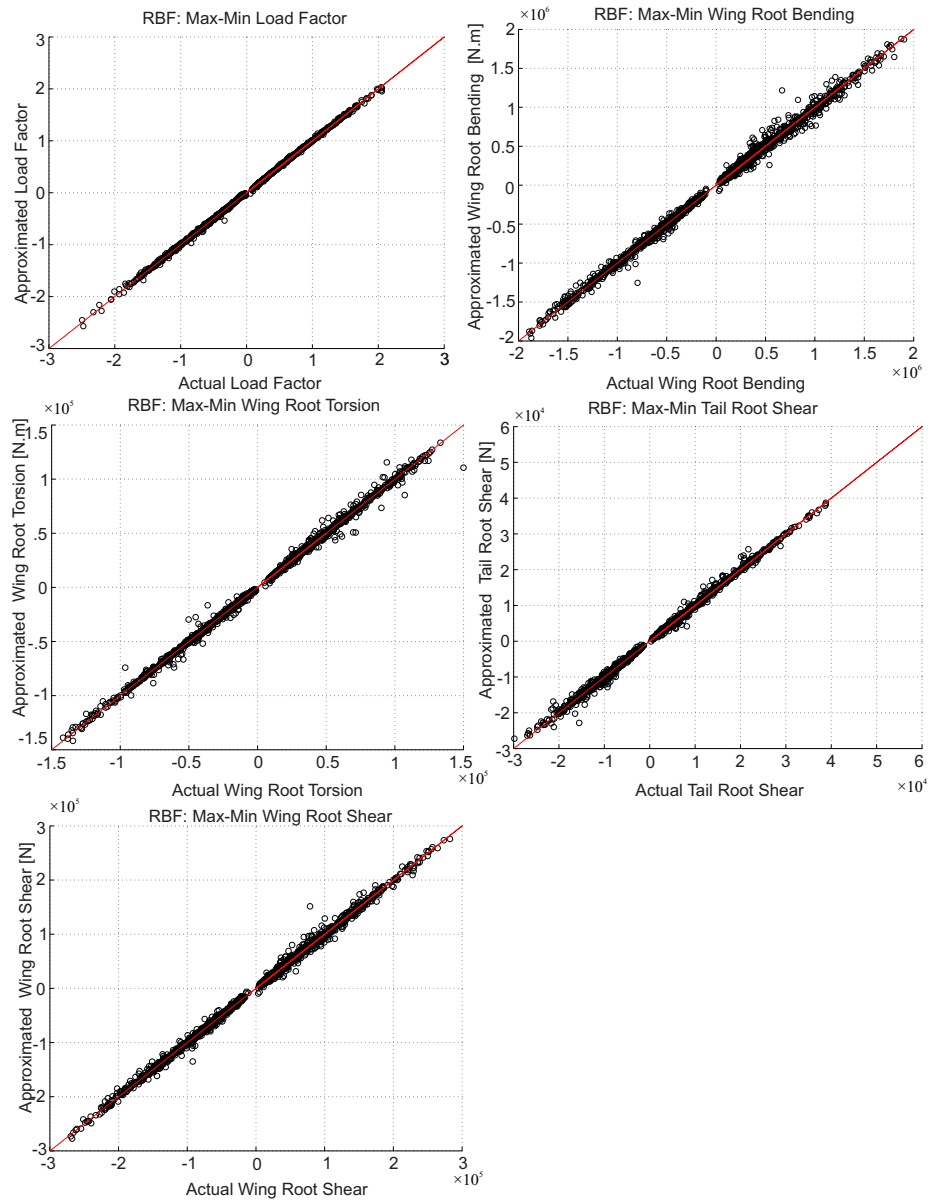


Figure 7: Correlation Plots for RBF-LH (600) results.

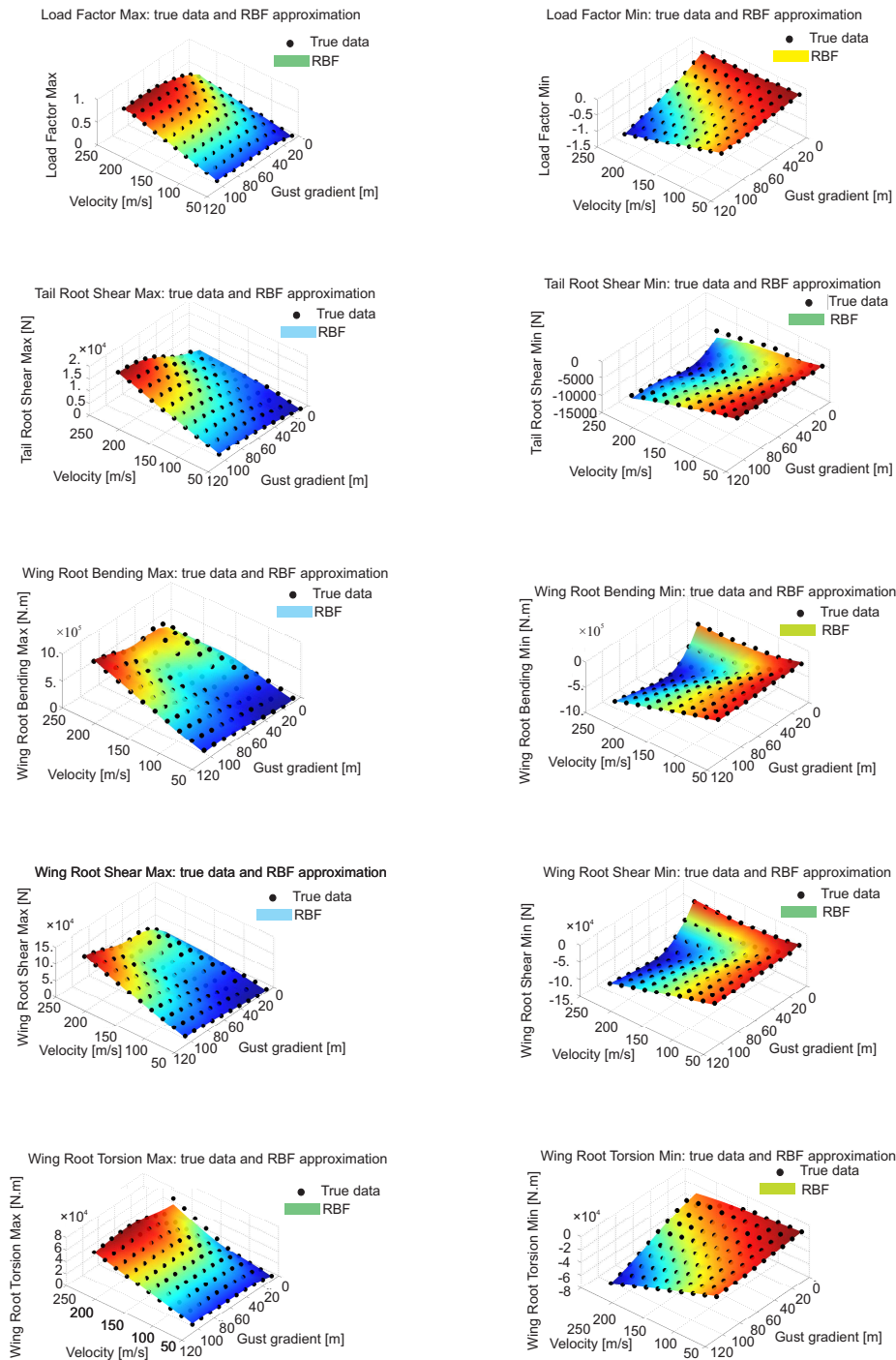


Figure 8: RBF Surfaces For LH 600 Sample Case.

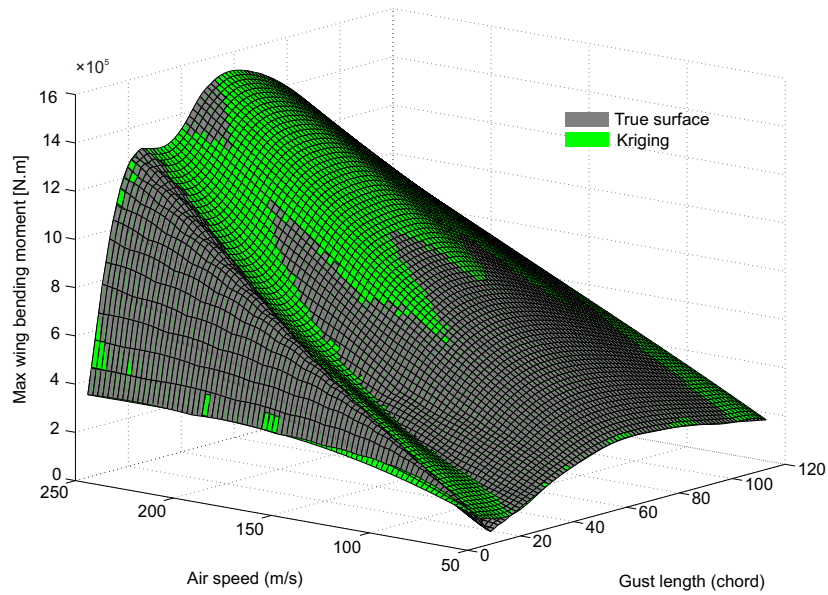


Figure 9: Maximum wing root bending moment versus gust length and air velocity.

sampling techniques may be used. In this case the optimal sampling method selected only 179 samples from the space of parameters variations, less than 25% of the previous sample size. The variation of maximum wing root torsion moment and minimum wing root shear force versus gust length and air velocity are shown in Figures 11 and 12. As it can be seen in the figures, the meta model constructed using optimal sampling is not a good global fit of the true function but the accuracy of the fit is significantly improved around the region with global maximum/minimum IQs. The optimisation results using the Kriging predictor presented in the next section show the advantage of using optimal sampling in finding the maximum and minimum values of IQs.

6. Optimization Approaches

In an effort to identify accurately the largest maximum and minimum values of the IQ responses for different flight conditions and configurations of the NLR model, the worst case approach was followed making use of a range of optimization methods. Taking into account that five gust output loads of the NLR model were considered for both the largest positive and negative values, ten separate optimization problems had to be solved.

All the worst case scenarios were solved using four alternative optimization methods. Three built-in optimizers of the ModelCenter software were invoked including a Hill-Climbing algorithm (Gradient Method) [19], an Evolutionary Algorithm (Darwin Method) and a hybrid approach (Design Explorer) which combines efficiently surrogate modeling and a gradient-based optimization method [19]. Moreover, the Bacterial Foraging Optimization Algorithm, which was used recently for aeroelastic tailoring [10], was also applied. The solution parameters of the Darwin Method were selected to be equivalent with the parameters of the BFO algorithm, corresponding to 20 genes and 100 generations. Due to the smooth shape of the search space, the gradient-based algorithms managed to converge towards the solution within few iterations in comparison with the bio-inspired methods, which used up all the iterations. The Gradient Method converged within 140 iterations in average for each worst gust case, while the Design Explorer converged within 75 iterations.

The exception to this pattern was the maximization case for the wing root torsion moment at which the evolutionary algorithms converged to the global

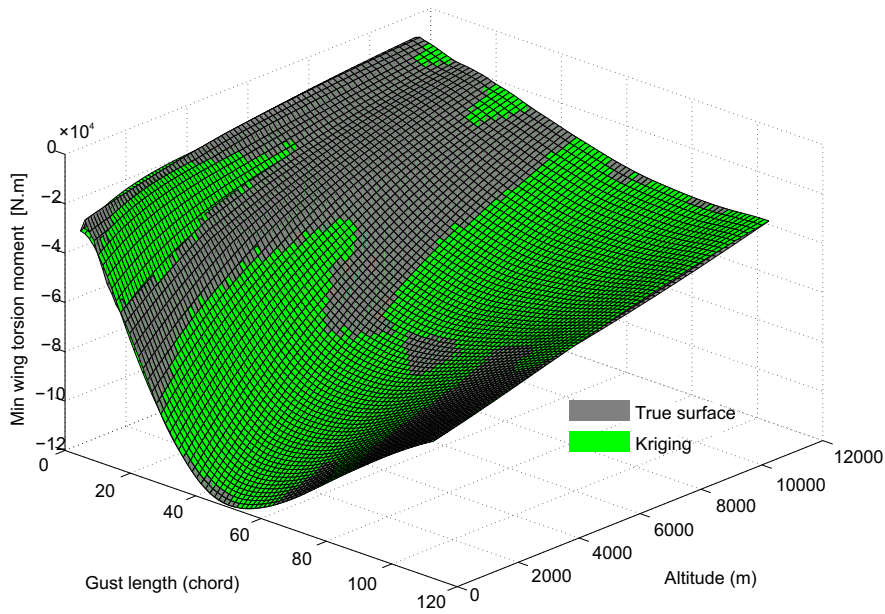


Figure 10: Minimum wing root torsion moment versus gust length and altitude.

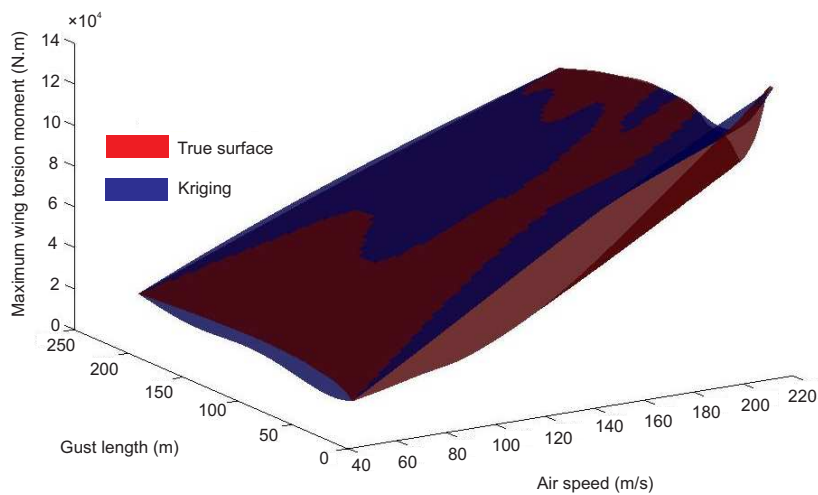


Figure 11: Maximum wing root torsion moment.

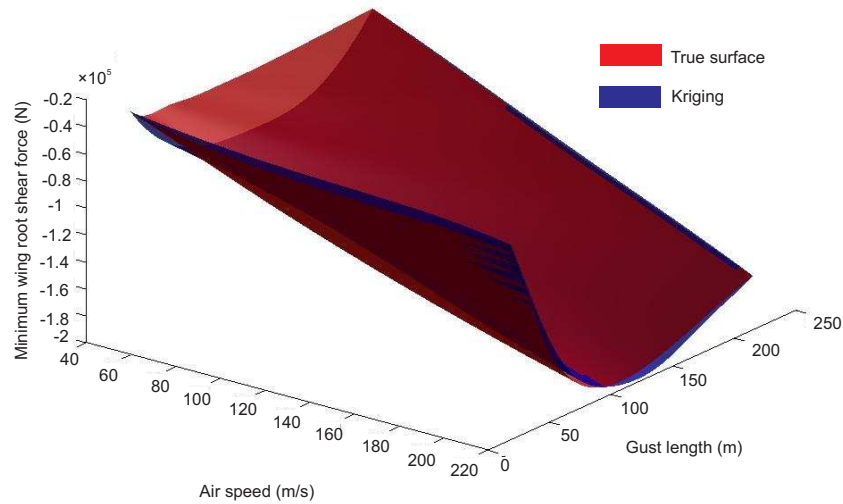


Figure 12: Minimum wing root shear force versus gust length and air velocity.

Table 4: Optimization results for the worst gust cases of the NLR model.

		cxcg	m [kg]	I _y [kgm ²]	L _g [m]	IQ
Load Factor [-]	Max	0.2	15000.0	1300000.0	145.75	2.64
	Min	0.1	15000.0	1300000.0	210.98	-3.19
Wing Root Shear Force [N]	Max	0.1	25000.0	1137481.2	214.0	381872.0
	Min	0.2	25000.0	1300000.0	117.21	-339064.5
Wing Root Bending Moment [Nm]	Max	0.1	25000.0	1170360.0	214.0	2539965.5
	Min	0.2	25000.0	1300000.0	98.91	-2392809.0
Wing Root Torsion Moment [Nm]	Max	0.2	22880.0	300000.0	19.3	177276.3
	Min	0.1	25000.0	1130463.8	214.0	-188652.1
Tail Root Shear Force [N]	Max	0.1	25000.0	1300000.0	177.65	52113.8
	Min	0.2	25000.0	1300000.0	79.8	-39088.0

optimum, while the gradient-based methods were trapped in a local maximum.

The best results obtained from the four optimization methods are summarized in Table 4. It is worth mentioning that for almost all the worst cases of the IQs (maximum and minimum) the first five design variables and more specifically the centre of gravity position, the half aircraft mass, the half aircraft moment of inertia, the true airspeed and the altitude reached the upper or lower limits. Furthermore, the true airspeed and the altitude were found to be 220 m/s and the sea level, respectively, for all the examined cases i.e. at the highest dynamic pressure. Additionally, the gust wavelength that leads to the largest values of the IQs responses was significantly different not only for the maximum and minimum cases of each quantity but as well as among all the quantities, as depicted more clearly at Figures 13 and 14. Finally, except from the load factor case and the wing root torsion moment case, the value of the maximum IQs was found to be larger than the corresponding absolute minimum value.

7. Genetic Algorithm Approaches

Genetic Algorithms attempt to mimic the Darwinian theory of natural selection, which is based upon the traits of the most successful animals being passed onto future generations. In an optimization setting [11], the characteristics of the best solutions from a range of initial estimates (genes) are passed onto subsequent iterations via a series of mathematical operators, which is repeated until convergence is achieved.

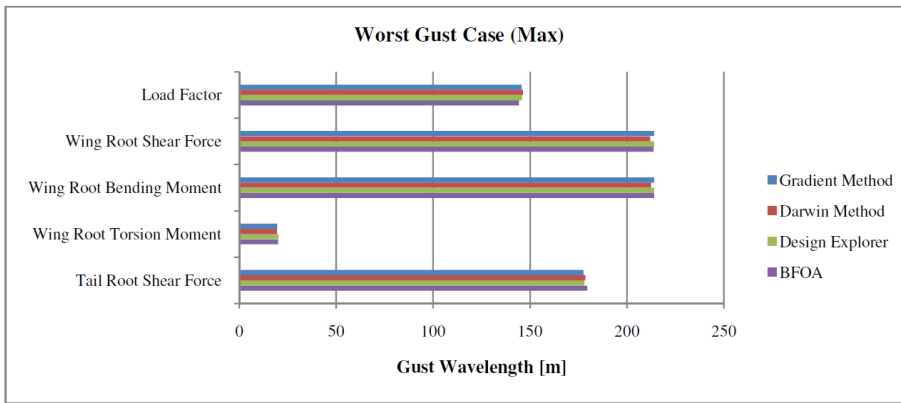


Figure 13: Gust wavelength for the worst gust cases (Max) using different optimization methods.

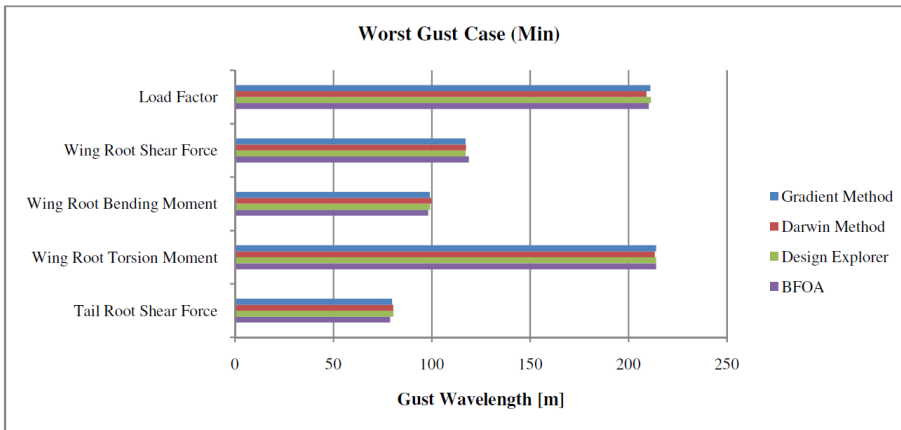


Figure 14: Gust wavelength for the worst gust cases (Min) using different optimization methods.

7.1 Binary Genetic Algorithm (BGA)

A common modeling of the genes parameters is achieved using a binary representation. Randomness is introduced via the application of a mutation, translation and crossover function as well as the inclusion of new blood solutions at each new iteration. An elitism parameter is also introduced.

Here, the binary representation of the variables and its subdivisions are listed in Table 5. For the implementation of the algorithm, a gene pool of 20 genes was used with the 2 best genes saved and 2 new-blood genes introduced each generation. A 90% probability of crossover, 10% probability of mutation, and a 20% likelihood of translation was used to generate each new generation. The optimization process was performed 10 times for all the different IQs. The best gene from each run is displayed in Figure 15 and the overall results are tabulated in Table 6 to Table 10 (Note: IQs are defined in Table 3).

Apart for the wing root bending moment, all the best solution have converged to the same value of the IQ under examination. The worst condition for load factor and the wing root torsion occur at sea level, maximum speed and with minimum weight. The difference is in the location of the centre of gravity. The load factor requires for the CoG to be as further aft as possible, while the wing root torsion moment the CoG is located as further forward as possible. The

Variable	Min	Max	Divisions
cxcg	0.1	0.2	16
Mass	15000	25000	16
Airspeed	50	330	16
Altitude	0	11000	16
Gust length	18	214	16

Table 5: Variable ranges and divisions (BGA).

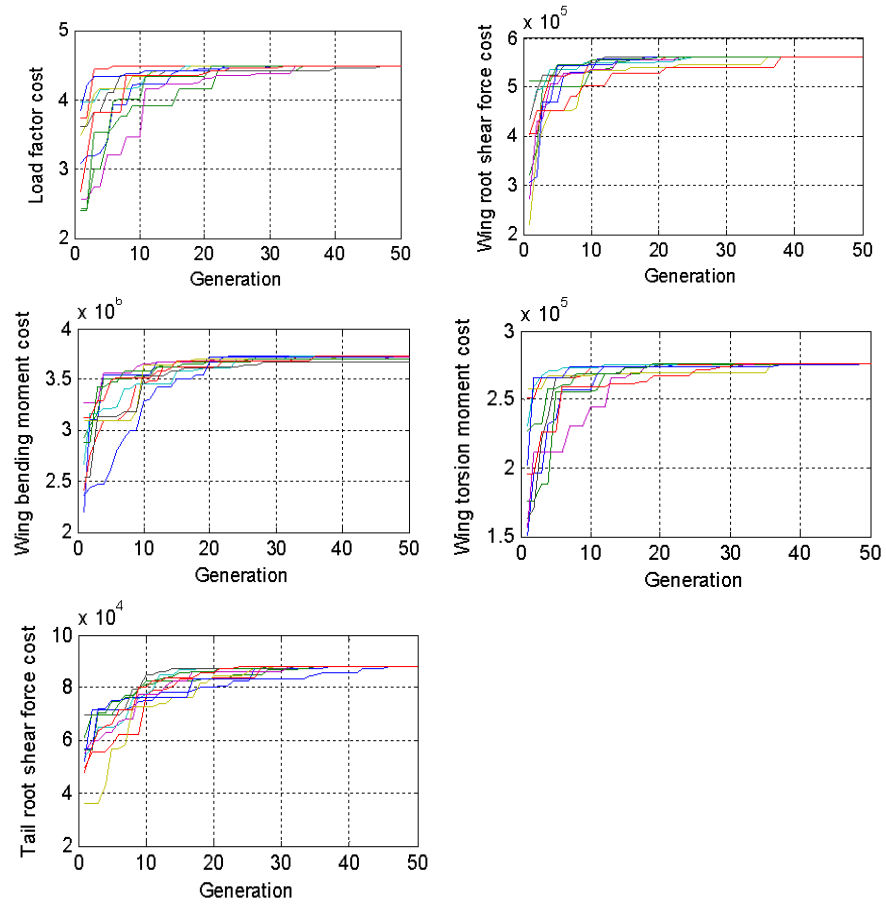


Figure 15: BGA Optimisation Trends.

Table 6: BGA Optimisation Result for Load Factor (sea level).

Run	cxcg	m kg	V m/s	IQ1	IQ2	IQ3 $\times 10^5$	IQ4 $\times 10^5$	IQ5 $\times 10^6$	IQ6 $\times 10^6$	IQ7 $\times 10^5$	IQ8 $\times 10^5$	IQ9 $\times 10^4$	IQ10 $\times 10^4$	Gust length	
														max	min
1	0.119	15000	330	3.72	-4.47	3.8259	-3.1275	2.8623	-2.4258	2.5781	-2.7630	7.3208	-4.5004	20.73	53.22
2	0.119	15000	330	3.72	-4.47	3.8259	-3.1275	2.8623	-2.4258	2.5781	-2.7630	7.3208	-4.5004	20.73	53.22
3	0.119	15000	330	3.72	-4.47	3.8259	-3.1275	2.8623	-2.4258	2.5781	-2.7630	7.3208	-4.5004	20.73	53.22
4	0.190	15000	330	3.74	-4.45	3.7983	-3.1935	2.8079	-2.4708	2.5782	-2.7508	7.2902	-4.4764	20.73	52.79
5	0.103	15000	330	3.71	-4.46	3.8284	-3.1120	2.8753	-2.4153	2.5779	-2.7658	7.3320	-4.6316	20.73	53.44
6	0.103	15000	330	3.71	-4.46	3.8284	-3.1120	2.8753	-2.4153	2.5779	-2.7658	7.3320	-4.6316	20.73	53.44
7	0.180	15000	330	3.74	-4.46	3.8042	-3.1848	2.8154	-2.4650	2.5782	-2.7524	7.3020	-4.4207	20.73	53.66
8	0.119	15000	330	3.72	-4.47	3.8259	-3.1275	2.8623	-2.4258	2.5781	-2.7630	7.3208	-4.5004	20.73	53.22
9	0.183	15000	330	3.74	-4.46	3.8024	-3.1877	2.8129	-2.4669	2.5782	-2.7519	7.2984	-4.4391	20.73	53.22
10	0.103	15000	330	3.71	-4.46	3.8284	-3.1120	2.8753	-2.4153	2.5779	-2.7658	7.3320	-4.6316	20.73	53.44

Table 7: BGA Optimisation Result for Wing Root Shear Force (sea level).

Run	cxcg	m kg	V m/s	IQ1	IQ2	IQ3 $\times 10^5$	IQ4 $\times 10^5$	IQ5 $\times 10^6$	IQ6 $\times 10^6$	IQ7 $\times 10^5$	IQ8 $\times 10^5$	IQ9 $\times 10^4$	IQ10 $\times 10^4$	Gust length	
														max	min
1	0.158	19921	330	2.84	-3.60	4.8605	-3.8708	3.3359	-2.7681	2.5823	-2.7256	8.1900	-4.9463	52.36	35.24
2	0.164	25000	330	2.27	-3.00	5.6155	-4.3357	3.6793	-2.9741	2.5822	-2.7079	8.7311	-5.4662	52.14	35.03
3	0.164	25000	330	2.27	-3.00	5.6155	-4.3357	3.6793	-2.9741	2.5822	-2.7079	8.7311	-5.4662	52.14	35.03
4	0.164	25000	330	2.27	-3.00	5.6155	-4.3357	3.6793	-2.9741	2.5822	-2.7079	8.7311	-5.4662	52.14	35.03
5	0.138	25000	330	2.27	-3.01	5.6257	-4.3033	3.6938	-2.9560	2.5829	-2.7114	8.7545	-5.6847	52.14	35.03
6	0.119	25000	330	2.26	-3.01	5.6287	-4.2786	3.7111	-2.9423	2.5834	-2.7141	8.7897	-5.8476	52.79	35.46
7	0.190	25000	330	2.28	-2.99	5.5962	-4.3764	3.6671	-2.9919	2.5815	-2.7045	8.6984	-5.5267	52.36	35.24
8	0.164	25000	330	2.27	-3.00	5.6155	-4.3357	3.6793	-2.9741	2.5822	-2.7079	8.7311	-5.4662	52.14	35.03
9	0.164	25000	330	2.27	-3.00	5.6155	-4.3357	3.6793	-2.9741	2.5822	-2.7079	8.7311	-5.4662	52.14	35.03
10	0.116	25000	330	2.26	-3.01	5.6286	-4.2745	3.7138	-2.9399	2.5834	-2.7145	8.7967	-5.8732	53.87	35.68

Table 8: BGA Optimisation Result for Wing root bending Moment (sea level).

Run	cxcg	m kg	V m/s	IQ1	IQ2	IQ3 $\times 10^5$	IQ4 $\times 10^5$	IQ5 $\times 10^6$	IQ6 $\times 10^6$	IQ7 $\times 10^5$	IQ8 $\times 10^5$	IQ9 $\times 10^4$	IQ10 $\times 10^4$	Gust length	
														max	min
1	0.1	25000	330	2.26	-3.01	5.6253	-4.25376	3.7256	-2.9283	2.5838	-2.7168	8.8286	-6.0229	49.11	30.04
2	0.151	25000	330	2.27	-3.01	5.6217	-4.31963	3.6835	-2.9651	2.5825	-2.7097	8.7458	-5.5730	49.32	30.04
3	0.1	19920.6	330	2.82	-3.60	4.9039	-3.80391	3.3676	-2.7288	2.5834	-2.7345	8.2860	-5.4316	49.11	30.04
4	0.1	25000	330	2.26	-3.01	5.6253	-4.25376	3.7256	-2.9283	2.5838	-2.7168	8.8286	-6.0229	49.11	30.04
5	0.112	25000	330	2.26	-3.01	5.6283	-4.2704	3.7163	-2.9376	2.5835	-2.7150	8.8034	-5.9004	49.76	30.04
6	0.1	25000	330	2.26	-3.01	5.6253	-4.2537	3.7256	-2.9283	2.5838	-2.7168	8.8286	-6.0229	49.11	30.04
7	0.1	25000	187.7	1.43	-1.83	3.1861	-2.9147	2.1198	-2.0871	1.3097	-1.5849	3.9946	-2.5989	48.89	29.83
8	0.1	25000	330	2.26	-3.01	5.6253	-4.2537	3.7256	-2.9283	2.5838	-2.7168	8.8286	-6.0229	49.11	30.04
9	0.1	22460.3	330	2.51	-3.28	5.2976	-4.0526	3.5662	-2.8394	2.5838	-2.7244	8.5903	-5.7577	49.11	30.04
10	0.1	25000	330	2.26	-3.01	5.6253	-4.2537	3.7256	-2.9283	2.5838	-2.7168	8.8286	-6.0229	49.11	30.04

Run	<i>cxcg</i>	<i>m</i> kg	<i>V</i> m/s	IQ1	IQ2	IQ3 ×10 ⁵	IQ4 ×10 ⁵	IQ5 ×10 ⁶	IQ6 ×10 ⁶	IQ7 ×10 ⁵	IQ8 ×10 ⁵	IQ9 ×10 ⁴	IQ10 ×10 ⁴	Gust length max	min
1	0.1	15000	330	3.71	-4.46	3.8288	-3.1088	2.8778	-2.4132	2.5779	-2.7663	7.3380	-4.6520	4.70	4.70
2	0.1	15000	330	3.71	-4.46	3.8288	-3.1088	2.8778	-2.4132	2.5779	-2.7663	7.3380	-4.6520	4.70	4.70
3	0.1	15000	330	3.71	-4.46	3.8288	-3.1088	2.8778	-2.4132	2.5779	-2.7663	7.3380	-4.6520	4.70	4.70
4	0.1	15000	330	3.71	-4.46	3.8288	-3.1088	2.8778	-2.4132	2.5779	-2.7663	7.3380	-4.6520	4.70	4.70
5	0.1	15000	330	3.71	-4.46	3.8288	-3.1088	2.8778	-2.4132	2.5779	-2.7663	7.3380	-4.6520	4.70	4.70
6	0.1	15000	330	3.71	-4.46	3.8288	-3.1088	2.8778	-2.4132	2.5779	-2.7663	7.3380	-4.6520	4.70	4.70
7	0.1	15000	330	3.71	-4.46	3.8288	-3.1088	2.8778	-2.4132	2.5779	-2.7663	7.3380	-4.6520	4.70	4.70
8	0.1	17539.6	330	3.19	-3.98	4.4453	-3.5112	3.1487	-2.5978	2.5820	-2.7473	7.8964	-5.0971	4.70	4.70
9	0.1	15000	330	3.71	-4.46	3.8288	-3.1088	2.8778	-2.4132	2.5779	-2.7663	7.3380	-4.6520	4.70	4.70
10	0.106	15000	330	3.71	-4.46	3.8280	-3.1151	2.8728	-2.4174	2.5779	-2.7652	7.3255	-4.6103	4.70	4.70

Table 9: BGA Optimisation Result for Wing Root Torsion Moment (sea level).

Run	<i>cxcg</i>	<i>m</i> kg	<i>V</i> m/s	IQ1	IQ2	IQ3 ×10 ⁵	IQ4 ×10 ⁵	IQ5 ×10 ⁶	IQ6 ×10 ⁶	IQ7 ×10 ⁵	IQ8 ×10 ⁵	IQ9 ×10 ⁴	IQ10 ×10 ⁴	Gust length max	min
1	0.151	25000	330	2.27	-3.01	5.6217	-4.3196	3.6835	-2.9651	2.5825	-2.7097	8.7458	-5.5730	38.28	60.15
2	0.1	22460	330	2.51	-3.28	5.2976	-4.0526	3.5662	-2.8394	2.5838	-2.7244	8.5903	-5.7577	38.06	60.15
3	0.1	25000	330	2.26	-3.01	5.6253	-4.2537	3.7256	-2.9283	2.5838	-2.7168	8.8286	-6.0229	38.28	60.15
4	0.151	25000	330	2.27	-3.01	5.6217	-4.3196	3.6835	-2.9651	2.5825	-2.7097	8.7458	-5.5730	38.28	60.15
5	0.1	25000	330	2.26	-3.01	5.6253	-4.2537	3.7256	-2.9283	2.5838	-2.7168	8.8286	-6.0229	38.28	60.15
6	0.1	25000	330	2.26	-3.01	5.6253	-4.2537	3.7256	-2.9283	2.5838	-2.7168	8.8286	-6.0229	38.28	60.15
7	0.1	25000	330	2.26	-3.01	5.6253	-4.2537	3.7256	-2.9283	2.5838	-2.7168	8.8286	-6.0229	38.28	60.15
8	0.1	22460	330	2.51	-3.28	5.2976	-4.0526	3.5662	-2.8394	2.5838	-2.7244	8.5903	-5.7577	38.06	60.15
9	0.112	25000	330	2.26	-3.01	5.6283	-4.2704	3.7163	-2.9376	2.5835	-2.7150	8.8034	-5.9004	38.71	60.59
10	0.125	25000	330	2.26	-3.01	5.6283	-4.2869	3.7057	-2.9469	2.5832	-2.7132	8.7741	-5.7950	38.49	60.37

Table 10: BGA Optimisation Result for Tail Root Shear Force (sea level).

other three IQs occur at sea level, maximum airspeed but at the maximum allowable weight. The worst condition for the tail shear force and wing root bending is achieved with the CoG as further forward as possible. The wing root shear force appears to achieve its worst condition with different CoG positions.

7.2 Continuous Genetic Algorithm (CGA)

Continuous, or real number, genetic algorithms work in a similar way to the BGA described above [11]. However, as the name suggests, the primary difference is in the variable representation of each gene. In CGA, the genes are represented using real numbers and consequently a re-definition of the mutation and crossover operators must be employed.

The mutation operator for CGA requires the selection of a number of variables on the basis of a mutation rate to be replaced by a new random variable. The best gene is left untouched, in order to give an element of elitism to the generation.

As for the BGA, a pair of genes is selected to create any offspring. For the BGA, if two points are selected and swapped, as here:

$$offspring_1 = [p_{11} \ p_{12} \ p_{13} \ p_{14} \ p_{15} \ p_{16} \ \dots \ p_{1N}] \quad (13)$$

$$offspring_2 = [p_{21} \ p_{22} \ p_{23} \ p_{24} \ p_{25} \ p_{26} \ \dots \ p_{2N}] \quad (14)$$

where N is the number of genes. By applying crossover (randomly chosen to occur after the second cell), the following offspring are obtained

$$offspring_1 = [p_{11} \ p_{12} \ p_{23} \ p_{24} \ p_{25} \ p_{16} \ \dots \ p_{1N}] \quad (15)$$

$$offspring_2 = [p_{21} \ p_{22} \ p_{23} \ p_{24} \ p_{15} \ p_{26} \ \dots \ p_{2N}] \quad (16)$$

It can be seen that no new information is passed to the offspring. However, for the CGA, new genetic material is introduced into the crossover process via the use of a blending function β , such that:

$$offspring_1 = parent_1 - \beta (parent_1 - parent_2) \quad (17)$$

where β is a random number between 0 and 1. In this application, a population of 20 genes was chosen, with the mutation rate set at 0.2 and the crossover rate at 0.5. The optimization process was performed 10 times for all the different IQs. The best gene from each run is displayed in Figure 16 and the overall results are tabulated in Table 11 to Table 15. It is evident from Figure 16 that

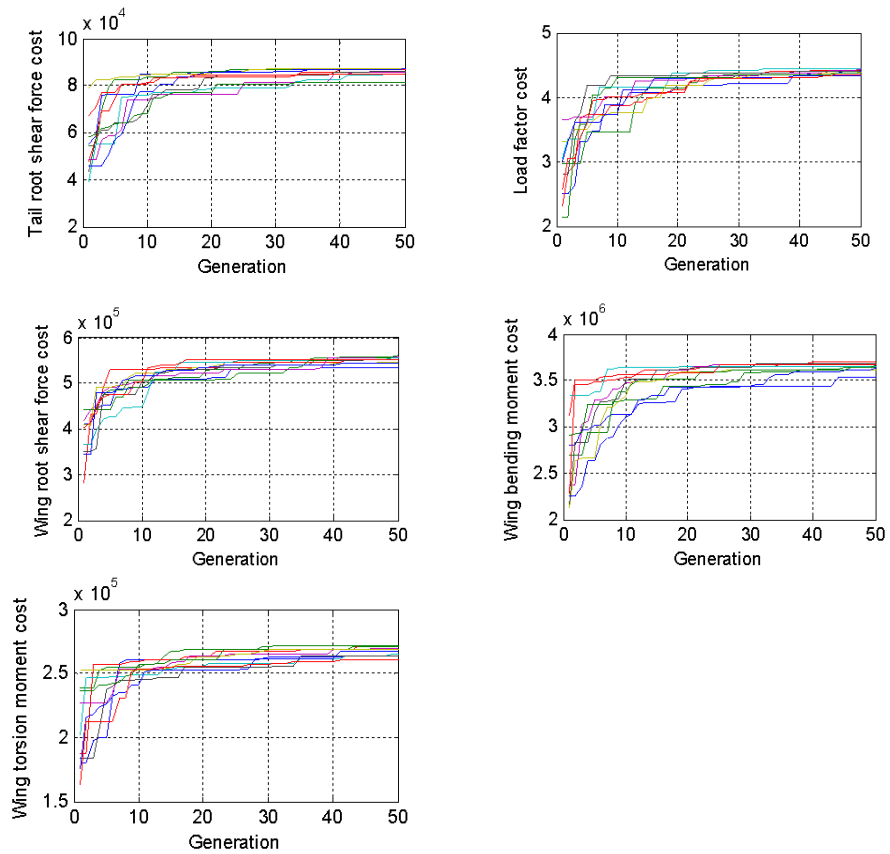


Figure 16: CGA Optimisation Trends.

Table 11: CGA Optimisation Result for Load Factor.

Run	<i>cxcg</i>	<i>m</i> kg	<i>V</i> m/s	<i>alt</i> m	IQ1	IQ2	IQ3 $\times 10^5$	IQ4 $\times 10^5$	IQ5 $\times 10^6$	IQ6 $\times 10^6$	IQ7 $\times 10^5$	IQ8 $\times 10^5$	IQ9 $\times 10^4$	IQ10 $\times 10^4$	Gust length	
															max	min
1	0.118	15179.4	328.3	59.2	3.63	-4.38	3.8377	-3.1309	2.8528	-2.4220	2.5513	-2.7091	7.2808	-4.4668	29.18	53.22
2	0.122	15001.2	328.7	186.0	3.63	-4.38	3.7444	-3.0656	2.7973	-2.3847	2.5050	-2.6541	7.1371	-4.3364	30.91	54.74
3	0.138	15006.3	327.7	43.2	3.68	-4.42	3.7869	-3.1207	2.8194	-2.4222	2.5555	-2.7076	7.2340	-4.2789	36.11	61.24
4	0.135	15036.4	329.7	77.4	3.68	-4.43	3.8003	-3.1242	2.8280	-2.4224	2.5485	-2.7185	7.2630	-4.3289	35.46	59.94
5	0.140	15029.2	328.6	48.0	3.68	-4.42	3.7988	-3.1306	2.8253	-2.4276	2.5563	-2.7170	7.2585	-4.2833	36.76	62.32
6	0.131	15110.3	328.9	120.1	3.63	-4.38	3.7981	-3.1155	2.8236	-2.4141	2.5304	-2.6868	7.2261	-4.3333	33.94	58.21
7	0.127	15190.4	328.6	1.4	3.66	-4.41	3.8633	-3.1614	2.8657	-2.4420	2.5740	-2.7398	7.3403	-4.4426	32.43	56.26
8	0.184	15194.4	325.3	107.8	3.60	-4.32	3.7458	-3.1574	2.7651	-2.4381	2.5241	-2.6336	7.0780	-4.3986	53.66	87.67
9	0.155	15197.6	329.8	115.6	3.63	-4.37	3.8226	-3.1592	2.8254	-2.4400	2.5348	-2.6966	7.2652	-4.2668	41.74	69.47
10	0.105	15061.4	327.4	192.9	3.59	-4.34	3.7510	-3.0508	2.8059	-2.3727	2.4990	-2.6364	7.1155	-4.4440	27.44	48.67

the optimization has failed to converge to a unique solution for any of the IQs. This indicates that more iterations are required in order to achieve convergence. Despite this limitation the CGA solution follow the same trends as for the BGA.

8. Optimisation using the Kriging Predictor

The Kriging meta-model constructed using optimal sampling method (section 5.2) can be used to find the maximum and minimum values of the 10 IQs with less computational time demand. The constrained optimisation technique based on Newton’s method, available in MATLAB (“*fmincon*”), is exploited in this case. The optimisations are also carried out on the true function for comparison

Table 12: CGA Optimisation Result for Wing Root Shear Force.

Run	<i>cxcg</i>	<i>m</i> kg	<i>V</i> m/s	<i>alt</i> m	IQ1	IQ2	IQ3 $\times 10^5$	IQ4 $\times 10^5$	IQ5 $\times 10^6$	IQ6 $\times 10^6$	IQ7 $\times 10^5$	IQ8 $\times 10^5$	IQ9 $\times 10^4$	IQ10 $\times 10^4$	Gust length	
															max	min
1	0.100	24879.7	324.3	362.3	2.14	-2.87	5.3317	-4.0543	3.5346	-2.7976	2.43206	-2.5434	8.2394	-5.5584	49.32	23.76
2	0.101	24786.6	327.7	20.4	2.26	-3.01	5.5670	-4.2060	3.6766	-2.9031	2.5691	-2.6763	8.6823	-5.9025	49.54	49.54
3	0.108	24938.9	328.6	163.4	2.22	-2.96	5.5132	-4.1713	3.6378	-2.8794	2.5182	-2.6193	8.5616	-5.7775	51.71	25.50
4	0.116	24987.5	328.3	104.4	2.23	-2.97	5.5481	-4.2078	3.6498	-2.9007	2.5388	-2.6412	8.6117	-5.7452	54.74	23.55
5	0.112	24835.0	328.6	4.3	2.27	-3.01	5.5909	-4.2397	3.6875	-2.9219	2.5775	-2.6938	8.7200	-5.8528	53.22	24.85
6	0.108	24832.4	324.0	133.3	2.20	-2.94	5.4518	-4.1557	3.6076	-2.8603	2.5142	-2.5991	8.4622	-5.6510	51.92	25.50
7	0.111	24922.7	328.3	110.5	2.23	-2.97	5.5378	-4.1947	3.6494	-2.8937	2.5369	-2.6397	8.5989	-5.7791	53.01	24.85
8	0.107	24982.1	327.0	288.9	2.17	-2.90	5.4262	-4.1111	3.5802	-2.8346	2.4670	-2.5728	8.3925	-5.6485	51.49	25.50
9	0.122	24852.3	329.8	5.7	2.27	-3.02	5.6045	-4.2678	3.6952	-2.9374	2.5805	-2.7085	8.7538	-5.7950	56.47	22.25
10	0.112	24941.1	329.7	140.3	2.23	-2.97	5.5380	-4.1987	3.6578	-2.8952	2.5299	-2.6441	8.6300	-5.7900	53.22	24.85

Run	cxcg	m kg	V m/s	alt m	IQ1	IQ2	IQ3 ×10 ⁵	IQ4 ×10 ⁵	IQ5 ×10 ⁶	IQ6 ×10 ⁶	IQ7 ×10 ⁵	IQ8 ×10 ⁵	IQ9 ×10 ⁴	IQ10 ×10 ⁴	Gust length	
															max	min
1	0.106	24755.0	324.2	343.8	2.16	-2.88	5.3239	-4.0602	3.5311	-2.8024	2.4383	-2.5442	8.2408	-5.5120	49.54	22.46
2	0.104	24523.2	329.4	145.0	2.26	-3.01	5.4788	-4.1528	3.6350	-2.8730	2.5274	-2.6395	8.5919	-5.8041	48.89	20.73
3	0.100	24763.1	329.1	7.3	2.27	-3.02	5.5847	-4.2251	3.6993	-2.9142	2.5785	-2.7024	8.7630	-5.9633	47.81	18.56
4	0.100	24898.8	326.5	71.7	2.23	-2.97	5.5373	-4.1801	3.6498	-2.8835	2.5459	-2.6350	8.5982	-5.8566	47.59	18.35
5	0.102	24898.1	327.7	20.2	2.25	-3.00	5.5812	-4.2152	3.6821	-2.9073	2.5691	-2.6761	8.6896	-5.9077	48.24	19.65
6	0.100	24715.2	325.8	142.5	2.22	-2.96	5.4639	-4.1347	3.6108	-2.8530	2.5171	-2.6027	8.4900	-5.7662	47.59	18.13
7	0.103	24947.9	329.6	64.8	2.25	-2.99	5.5799	-4.2204	3.6916	-2.9089	2.5580	-2.6796	8.7276	-5.9237	48.46	20.08
8	0.131	24849.7	326.9	68.8	2.24	-2.98	5.5292	-4.2300	3.6423	-2.9070	2.5475	-2.6380	8.5960	-5.5893	58.21	20.30
9	0.101	24775.7	329.6	108.0	2.25	-2.99	5.5333	-4.1871	3.6670	-2.8908	2.5419	-2.6596	8.6678	-5.8856	48.02	19.00
10	0.105	24985.8	325.8	17.4	2.23	-2.97	5.5687	-4.2149	3.6699	-2.8992	2.5636	-2.6494	8.6482	-5.8455	49.32	21.81

Table 13:
CGA Op-
timisation
Result for
Wing root
bending
Moment.

Run	cxcg	m kg	V m/s	alt m	IQ1	IQ2	IQ3 ×10 ⁵	IQ4 ×10 ⁵	IQ5 ×10 ⁶	IQ6 ×10 ⁶	IQ7 ×10 ⁵	IQ8 ×10 ⁵	IQ9 ×10 ⁴	IQ10 ×10 ⁴	Gust length	
															max	min
1	0.110	15107.6	327.1	178.0	3.58	-4.33	3.7648	-3.0665	2.8098	-2.3818	2.5037	-2.6383	7.1329	-4.4203	26.80	51.49
2	0.100	15209.7	328.8	77.0	3.62	-4.37	3.8451	-3.1165	2.8695	-2.4110	2.5461	-2.7103	7.2796	-4.6053	25.71	48.02
3	0.105	15385.5	327.2	17.3	3.59	-4.34	3.9014	-3.1620	2.8895	-2.4357	2.5643	-2.7155	7.3419	-4.6004	26.36	49.76
4	0.109	15011.8	324.2	58.7	3.62	-4.36	3.7549	-3.0690	2.8061	-2.3869	2.5385	-2.6555	7.1306	-4.4118	26.80	51.27
5	0.112	15284.4	327.6	55.8	3.60	-4.35	3.8623	-3.1412	2.8656	-2.4253	2.5509	-2.7021	7.2942	-4.5187	26.80	52.14
6	0.100	15972.3	325.1	3.6	3.44	-4.20	4.0308	-3.2449	2.9450	-2.4707	2.5637	-2.6883	7.4320	-4.7057	25.71	48.02
7	0.104	15024.8	329.0	221.7	3.60	-4.36	3.7426	-3.0430	2.8068	-2.3684	2.4925	-2.6433	7.1152	-4.4592	26.36	49.32
8	0.118	15007.9	329.6	167.4	3.64	-4.39	3.7615	-3.0735	2.8146	-2.3894	2.5145	-2.6764	7.1750	-4.3969	26.15	53.87
9	0.104	15429.6	328.8	55.2	3.58	-4.34	3.9111	-3.1647	2.8965	-2.4353	2.5547	-2.7179	7.3551	-4.6298	26.36	49.32
10	0.100	15353.9	321.2	77.9	3.50	-4.25	3.7967	-3.0926	2.8200	-2.3889	2.5220	-2.6036	7.0999	-4.4480	25.71	48.01

Table 14:
CGA Op-
timisation
Result for
Wing Root
Torsion
Moment.

purposes. Results obtained from optimisation methods are shown in Table 16. It can be seen in the table that the optimisation results obtained from Kriging Meta models are in good agreement with their corresponding true values. The maximum error of Kriging IQs of 6.9 % indicating the accuracy of the Kriging model around the maximum/minimum points. However the accuracy can be increased by constructing a new meta-model on a small region around the optimum point of the parameters (the points obtained from the optimisation procedure on Kriging meta-model) and repeat the optimisation procedure. Note that the smaller ranges of parameters variations often lead to better fitted surfaces. Errors in the optimum parameters shown in Table 16 show that the optimisations on Kriging model in most cases converge to the true optimum points (or at least very close to them). However in one case (Maximum wing root torsion moment) the converged parameter of the aircraft mass using Kriging model is quite far from its true optimum values. This is due to the fact that this IQ (Maximum wing root torsion moment) is not sensitive to the mass parameter as the variation of the IQ due to variation of mass over its whole range (15e3 – 25e3 kg) is less than 2%.

9. Conclusions

A number of different Design of Experiments, surrogate modeling and optimization techniques have been applied to "1-cosine" gust response data from a simple assumed modes free-free aircraft model with 5 "interesting quantities". It has been shown that using these data sets, it is possible to deduce accurate surrogate models for the worst case gust loads using relatively few design test cases compare to a full scale Monte-Carlo investigation. Further investigation is required to determine the best approach and also the number of test samples to use. These encouraging initial results will be built upon in future studies as part of the FFAST FP7 research programme in order to assess whether the methodologies are applicable to full scale aircraft models with many modes and nonlinear features, as well as large numbers of "interesting quantities".

Run	cxcg	m kg	V m/s	alt m	IQ1	IQ2	IQ3 ×10 ⁵	IQ4 ×10 ⁵	IQ5 ×10 ⁶	IQ6 ×10 ⁶	IQ7 ×10 ⁵	IQ8 ×10 ⁵	IQ9 ×10 ⁴	IQ10 ×10 ⁴	Gust length	
															max	min
1	0.101	24904.9	329.7	64.4	2.25	-3.00	5.5747	-4.2150	3.6923	-2.9063	2.5586	-2.6813	8.7329	-5.9476	30.69	4.70
2	0.102	24766.0	329.2	28.8	2.27	-3.02	5.5729	-4.2165	3.6905	-2.9090	2.5703	-2.6915	8.7359	-5.9367	31.13	4.70
3	0.104	24895.1	329.6	78.9	2.25	-3.00	5.5656	-4.2113	3.6835	-2.9040	2.5529	-2.6733	8.7079	-5.9040	31.99	4.70
4	0.108	24179.5	327.8	144.5	2.29	-3.04	5.4185	-4.1144	3.5909	-2.8544	2.5226	-2.6182	8.4791	-5.6954	33.73	4.70
5	0.104	24995.5	323.1	17.4	2.21	-2.95	5.5253	-4.2052	3.6530	-2.8892	2.5540	-2.6298	8.5771	-5.7673	31.99	4.70
6	0.100	24833.4	329.5	34.9	2.27	-3.01	5.5802	-4.2201	3.6967	-2.9103	2.5690	-2.6926	8.7507	-5.9611	30.48	4.70
7	0.110	24997.4	329.9	160.7	2.22	-2.96	5.5348	-4.1922	3.6572	-2.8907	2.5229	-2.6365	8.6234	-5.8025	34.38	4.70
8	0.104	24941.7	329.9	82.7	2.25	-2.99	5.5718	-4.2168	3.6879	-2.9065	2.5523	-2.6753	8.7196	-5.9104	31.99	4.70
9	0.101	24808.3	322.8	428.3	2.12	-2.85	5.2553	-4.0168	3.4939	-2.7754	2.4034	-2.5175	8.1169	-5.4532	31.13	4.70
10	0.103	24807.4	321.0	37.0	2.21	-2.95	5.4507	-4.1728	3.6160	-2.8720	2.5390	-2.6094	8.4740	-5.6771	31.78	4.70

Table 15:
CGA Op-
timisation
Result
for Tail
Root Shear
Force.

Table 16: True and predicted maximum/minimum values of 5 IQs and their corresponding input parameters.

		cxcg	m (kg)	V (m/s)	alt (m)	I_y (N.m ²)	L_g (m)	IQ	Error IQ (%)
IQ1	True	0.2	15e3	220	0	8.16e5	133.82	2.06	
	Kriging	0.17	15e3	220	0	8.17e5	133.12	2.02	-2.14
	Errors in parameters (%)	-16.0	0	0	0	0.03	-0.53		
IQ2	True	0.10	16e3	220	0	1.3e6	214	-2.40	
	Kriging	0.109	15e3	220	0	1.22e6	205.9	-2.57	6.9
	Errors in parameters (%)	9.3	-8.7	0	0	-5.84	-3.79		
IQ3	True	0.10	25e3	220	0	1.14e6	214.00	3.05e5	
	Kriging	0.104	25e3	220	0	1.15e6	212.48	3.06e5	0.11
	Errors in parameters (%)	4.4	0	0	0	1.31	-0.71		
IQ4	True	0.2	25e3	220	0	1.3e6	117.21	-2.71e5	
	Kriging	0.13	25e3	220	0	1.12e3	122.73	-2.66e5	1.88
	Errors in parameters (%)	32.6	0	0	0	13.92	-4.71		
IQ5	True	0.10	25e3	220	0	1.18e6	214	2.03e6	
	Kriging	0.105	25e3	220	0	1.14e6	209.5	2.04e6	0.31
	Errors in parameters (%)	4.86	0	0	0	-2.81	-2.11		
IQ6	True	0.20	25e3	220	0	1.3e6	98.91	-1.91e6	
	Kriging	0.18	25e3	220	0	1.1e6	93.32	-1.88e6	1.47
	Errors in parameters (%)	10.6	0	0	0	13.94	5.65		
IQ7	True	0.10	15e3	220	0	1.3e6	19.57	1.38e5	
	Kriging	0.10	25e3	220	0	1.3e6	18.0	1.36e5	-0.94
	Errors in parameters (%)	0	66.7	0	0	0	-8.01		
IQ8	True	0.10	25e3	220	0	1.13e6	214	-1.51e5	
	Kriging	0.10	24.9e3	220	0	1.18e6	214	-1.51e5	-0.06
	Errors in parameters (%)	0	-0.22	0	0	4.26	0		
IQ9	True	0.10	25e3	220	0	1.3e6	177.65	4.17e4	
	Kriging	0.12	25e3	220	0	1.1e6	152.86	4.12e4	0.91
	Errors in parameters (%)	15.8	0	0	0	15.6	13.96		
IQ10	True	0.20	25e3	220	0	1.3e6	79.8	-3.12e4	
	Kriging	0.18	25e3	220	0	1.26e6	72.77	-3.0e4	-3.99
	Errors in parameters (%)	-8.98	0	0	0	-3.44	-8.80		

10. Acknowledgments

The research leading to these results has received funding from the European Community's Seventh Framework Programme (FP7 / 2007-2013) under a grant agreement number 233665. FFAST (Future Fast Aeroelastic Simulation Technologies) is a collaborative research project aimed at developing, implementing and assessing a range of numerical simulation technologies to accelerate future aircraft design. Advances in critical load identification and reduced order modelling methods will potentially provide a step change in the efficiency and accuracy of the dynamic aeroelastic loads process. The partners in FFAST are: University of Bristol, INRIA, CSIR, TU Delft, DLR, IRIAS, University of Liverpool, Politecnico di Milano, NUMECA, Optimad Engineering, Airbus-UK, EADS-MS and IITP.

This work is also partially supported through the Virtual Engineering Centre (VEC), which is a University of Liverpool initiative in partnership with the Northwest Aerospace Alliance, the Science and Technology Facilities Council (Daresbury Laboratory), BAE Systems, Morson Projects and Airbus (UK). The VEC is funded by the Northwest Regional Development Agency (NWDA) and European Regional Development Fund (ERDF) to provide a focal point for virtual engineering research, education and skills development, best practice demonstration, and knowledge transfer to the aerospace sector.

References

- [1] W. Chen. *A Robust Concept Exploration Method for Configuring Complex System*. PhD thesis, Mechanical Engineering, Georgia Institute of Technology, Atlanta, GA, 1995.
- [2] N. Cressie. Spatial prediction and ordinary kriging. *Mathematical Geology*, 20(4):405-421, 1988.
- [3] D. Dimitriadis and J. E. Cooper. "Gust Loads", Chapter 4. in "Design Loads for Future Aircraft". RTOTR045., 1993.
- [4] N. Dyn, D. Levin, and S. Rippa. Numerical procedures for surface fitting of scattered data by radial basis functions. *SIAM Journal of Scientific and Statistical Computing*, 7(2):639-659, 1986.
- [5] A. Forrester et al. *Engineering Design via Surrogate Modelling: A Practical Guide*. Wiley, 2008.
- [6] H. Fang and M. F. Horstemeyer. Global response approximation with radial basis functions. *Journal of Engineering Optimization*, 38(4):407-424, 2006.
- [7] J. R. Flomenhoft. Brief history of gust models for aircraft design. *Journal of Aircraft*, 31(5):1225-1227, 1994.
- [8] J. H. Friedman. Multivariate adaptive regressive splines. *The Annals of Statistics*, 19(1):1-67, 1991.
- [9] J. R. Fuller. Evolution of airplane gust loads design requirements. *Journal of Aircraft*, 32(2):235-246, 1995.
- [10] Georgiou G. and Cooper J.E. Aeroelastic tailoring using bacterial foraging optimisation. In *Proceedings of 8th Conference of the Association for Structural and Multidisciplinary Optimization in the UK*, London, United Kingdom, 2010.
- [11] R. L. Haupt and S. E. Haupt. *Practical genetic algorithms, 2nd ed.* Chichester. Wiley Interscience, 2004.

- [12] F.M. Hoblit. *Gust Loads on Aircraft - Concepts and Applications*. AIAA, 1988.
- [13] E.H. Isaaks and R.M. Srivastava. *An Introduction to Applied Geostatistics*. Oxford University Press, 1989.
- [14] D. R. Jones, M. Schonlau, and W. J. Welch. Efficient global optimization of expensive black-box functions. *Journal of Global Optimization*, 13(4):455–492, 1998.
- [15] T.L. Lomax. *Structural Loads Analysis for Commercial Transport Aircraft: Theory and Practice*. AIAA Education Series, 1996.
- [16] S.N. Lophaven, H.B. Nielsen, and J. Sondergaard. Dace, a matlab kriging toolbox. Technical Report I MM-TR-2002-12, Technical University of Denmark, DK-2800 Kgs. Lyngby Denmark, 2002.
- [17] R. H. Myers and D. Montgomery. *Response Surface Methodology: Process and Product Optimization Using Designed Experiments*. John Wiley and Sons, 2008.
- [18] M. Papadrakakis, M. Lagaros, and Y. Tsompanakis. Structural optimization using evolution strategies and neural networks. *Computer Methods in Applied Mechanics and Engineering*, 156(1-4):309–333, 1998.
- [19] Phoenix Integration Inc., Blacksburg, Virginia. *ModelCenter v9.0, Design Process Optimization Software*, 2010.
- [20] J. Sacks, S. B. Schiller, and W. J. Welch. Designs for computer experiments. *Technometrics*, 31, 1989.
- [21] J. Sacks, W. J. Welch, T. J. Mitchell, and H. P. Wynn. Design and analysis of computer experiments. *Statistical Science*, 4(4):409–435, 1989.
- [22] W. J. Vink. and J. B. de Jonge. A matlab program to study gust loading on a simple aircraft model. Technical Report NLR TP 97379 1997, National Aerospace Laboratory NLR, Amsterdam, The Netherland, 1997.
- [23] J. R. Wright and J. E. Cooper. *Introduction to Aircraft Aeroelasticity and Loads*. Wiley, 2007.